Saturation of influenza virus neutralization and antibody consumption can both lead to bistable growth kinetics

Shilian Xu[a], Ada W. C. Yan[b], Heidi Peck[c], Leah Gillespie[c], Ian Barr[c], Xiaoyun Yang[d], Stephen Turner[a], Celeste M Donato[a,e], Tonghua Zhang[f], Moshe Olshansky[a,g], Dhanasekaran Vijaykrishna[a,c,1]

[a]Department of Microbiology, Biomedicine Discovery Institute, Monash University, Clayton VIC 3800, Australia

[b]MRC Centre for Global Infectious Disease Analysis, Department of Infectious Disease Epidemiology, School of Public Health, Imperial College London, London W21PG, United Kingdom.

[c]World Health Organization Collaborating Centre for Reference and Research on Influenza, Peter Doherty Institute for Infection and Immunity, Melbourne VIC 3000, Australia.

[d]State Key Laboratory for Respiratory Disease, Guangdong Medical University, Guangzhou Guangdong 511436, China PR

[e]Enteric Diseases Group, Murdoch Children's Research Institute, Parkville VIC 3052, Australia

[f]Department of Mathematics, Swinburne University of Technology, Hawthorn VIC 3122, Australia

[g]Baker Heart and Diabetes Institute, Melbourne VIC 3004, Australia

[1]Email: vijay.dhanasekaran@monash.edu

ABSTRACT

The efficacy of antibody-dependent vaccines relies on both virus replication and neutralisation, but their quantitative relationship is unknown. To bridge this gap, we investigated the growth of avian and human influenza viruses, and the virus neutralisation by antibodies *in vitro*. A one-dimensional deterministic model accurately predicted the growth of avian and human influenza in cell culture, and neutralisation of seasonal influenza viruses determined using focus reduction assay. According to this model, at a specific interval of antibody concentration, viruses can either survive or die due to bistability, where small viral inocula are eliminated but not large virus inocula; this is caused by saturated virus neutralization or antibody consumption. Our finding highlights the importance of inoculum size even when virus-antibody pair is well-matched and provides a possible mechanism for high influenza re-infections and low vaccine efficacy, thereby facilitating the formulation of strategies to enhance the efficacy of influenza vaccines and antiviral treatments.

KEYWORDS:

Antibody neutralization, influenza virus, bistable growth kinetics, antibody saturation

Introduction

Eliciting a neutralizing antibody response is the primary goal of vaccination which commonly correlates with protection from disease. Owing to its importance, neutralization by antibodies has been studied extensively for several viruses (*1-6*). Neutralization of acute viral infections, such as influenza, results from pre-existing antibodies, elicited through prior infection or immunization, whereby the virion surface is coated by pre-existing antibodies to interfere with viral attachment or release (*7*). As viral surfaces are readily available for antibody binding, neutralization occurs through antibody binding at “critical binding sites” (*7*). For viruses such as influenza binding to the right location (“single-hit”) is adequate for neutralization, and can be diminished by affinity and avidity of antibodies (*8*); while the “multiple-hit” model requires several antibody molecules for neutralization (*9*).

The survival or eradication of virus is dependent on the rate of neutralization, since the effective rate of neutralization is affected both by viral replication and the capacity of antibodies to neutralize the viruses, however the rate of virus growth through replication and the rate of neutralization is often overlooked or entirely ignored in models and *in vitro* studies.

Simple compartmental models have been used to provide a great deal of understanding of the within-host kinetics of viral infection (*10-15*), and have played a key role in quantifying pre-existing immunity (*16, 17*). In existing within-host models of virus-antibody interaction, rate of virus neutralization is assumed to increase infinitely with increase of viral titre or antibody concentration (*13, 14, 18*), thereby ignoring saturation. Saturation commonly occurs in biological systems; whose effects are

innately nonlinear in proportion to reactant concentrations (*19-21*). Crucially, saturation always leads to a bistable behaviour – biologically known as the inoculum effect, shown in Fig.1, whereby at the same antibody concentration interval, viruses can either survive or die (*22-25*). It is unclear whether the oversimplified model of unsaturated virus neutralization can capture this behaviour.

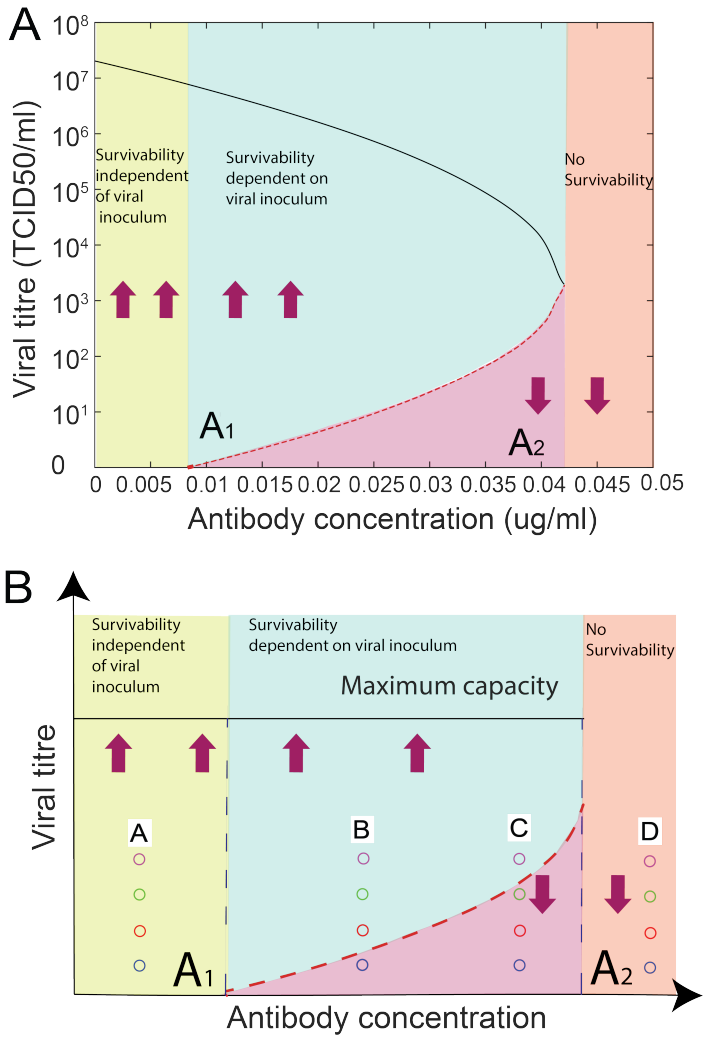

Figure 1. Saturation leads to antibody-induced bistable viral kinetics at antibody concentration interval, A1 and A2. Virus survives if viral inoculum is above dashed red curve and is inhibited if viral inoculum is below dashed red curve. Purple arrows represent any viral inoculum size. Bistable viral kinetics are classified into two categories. A) The maximal capacity of viral titre decreases with increase of antibody concentration. B) The viral titre survives and converges to the same maximal capacity independent of antibody concentration (schematic diagram).

Protection against virus infection can be diminished by a diverse set of neutralization escape mechanisms, including antigenic variation, where escape mutants predominate infections, as well as by host exposure history, described invariably through antigenic sin (*26*), seniority (*27*), or imprinting (*28*). Some of these limitations, specifically for highly diverse pathogens such as influenza, can be potentially overcome by the recent focus on the development of broadly reacting universal vaccines (*29, 30*). However, our current understandings of virus-host interactions do not fully explain poor rates of protection and high rates of re-infection.

Re-infection is commonly observed among several endogenous viruses (e.g. herpes simplex complex) and exogenous viruses that cause transient infection, however re-infections due to the same genotype are particularly common and well-characterized in acute respiratory viral diseases (*31*). More than 25% re-infection is observed in Respiratory Syncytial Virus genotypes (*32-34*), whereas 9-25% re-infection has been described for various influenza virus types: 17% re-infection was observed among seasonal influenza A/H3N2 infected students during the same season in 1970; whereas 9.3% and 20% re-infection rates were observed for A/H1N1 in 1980 (*35*). A recent sequential challenge experiment with the 2009 pandemic virus A/H1N1pdm09 suggested that re-infection may not be rare (*36*). These studies collectively suggest that pre-existing immunity alone cannot guarantee exemption of future infection.

In this study, we demonstrate the potential importance of antibody-induced bistable virus kinetics using the influenza virus as an example, a major human health concern responsible for an estimated 290,000 – 650,000 deaths annually (*37, 38*). The evolutionary history and epidemiology of influenza is closely linked to its ability to evade

70 pre-existing immune responses that most humans acquire though vaccination and prior
71 infection (*39*). Despite advances in our understanding of pre-existing immunity, provided
72 by immune memory cells, particularly memory T and B cells, and strain specific
73 antibodies (*40*), antibody mediated influenza vaccine is generally less than 60%
74 effective in protecting individuals against influenza infection (*39*). To achieve the NIH
75 goal of 75% universal vaccine protection against influenza a better understanding of
76 correlates of protection against influenza is required (48, 49). The ability of host serum
77 to block hemagglutination of influenza virus, through the hemagglutination inhibition
78 assay (HAI), is accepted as a reasonably accurate correlate of protection by many
79 regulatory agencies (*39, 41*). However, unlike the virus neutralization assays, such as
80 the plaque reduction assay (also known as focus reduction assay or FRA), HAI does not
81 take viral replication kinetics into consideration and thereby providing no information on
82 neutralized viral titre, suggesting that virus neutralization kinetics is poorly understood.
83 To understand how saturation of virus neutralization affects viral kinetics, we
84 propose a class of two-dimensional deterministic models involving only virus replication
85 and virus neutralization that are relatively easy to directly measure. First, using a one-
86 dimensional deterministic model we show that virus replication converges to a
87 maximum capacity independent of viral inoculum sizes. Next, by fitting focus reduction
88 assays (FRA) performed for seasonal influenza A/H3N2 viruses circulating during
89 2014–2019 and using ferret antisera raised against a representative set of A/H3N2
90 viruses, we obtain parameters for virus neutralization by antibody binding, and found
91 that saturated virus neutralization is more accurate and robust than unsaturated virus
92 neutralization. Integrating replication and neutralization parameters into the proposed

93 deterministic models, we identified saturated virus neutralization or antibody
94 consumption leads to bistable viral kinetics in the presence of neutralizing antibodies. In
95 sum, our results show that even for well-matched antibody-virus pair, neutralization can
96 be diminished by not only the antibody concentration but also the virus inoculum size,
97 implying that variability of virus neutralization can be caused by saturated virus
98 neutralization and antibody consumption are biological features of the interaction
99 between virus and antibody.

Results

Influenza virus converges to maximal capacity on A549 cells obeying one-dimensional growth kinetics.

To understand the role of viral inoculum size (i.e. initial viral load) on viral replication kinetics we used previously published influenza virus growth assays performed in the absence of antibodies (*42*). Since, in the absence of antibodies influenza replication *in vitro* and *in vivo* is solely limited by the availability of susceptible cells (*12, 42, 43*), we describe the change of virus titre through natural virus replication and degradation in limited number of susceptible cells as $\frac{dV(t)}{dt} = \frac{\rho V(t)}{1+\beta V(t)} - \sigma V(t)$, (1). This system is illustrated by the green terms in Fig. 2. $V(t)$ represents viral titre with respect to time t. Parameters ρ represents replication rate of influenza virus; β controls natural saturation of viral replication at high viral titer; σ represents degradation rate of influenza virus. We believe that stochastic effects may not play a decisive role supporting the usage of ordinary differential equation (ODE) models, as viral titres are considerably large during both clinical and experimental infection (in the range of $10^6 \sim 10^8\, TCID50/ml$) (*12, 42, 44, 45*), although stochasticity may affect the steady state reached from a given initial condition, such as if early extinction of the virus occurs.

We fit Eq. 1 to single-cycle (SC) and multiple-cycle (MC) infection assay of A/H1N1pdm09 and avian influenza A/H7N9 viruses, performed by Simon *et al*. (*42*), using the combined sum of squared error (combined SSE) (Fig. 3). The SC assay was performed with infection at high viral multiplicity of infection (MOI), 3 plaque forming unit (PFU)/cell, such that 95% of the cells were infected simultaneously, whereas the MC assay was performed with infection at low MOI (0.01 PFU/cell) such that only a small

123 population of cells were infected and new viral progeny are continuously generated.

124 Thus, SC and MC assays provide viral replication kinetics with different inoculum sizes.

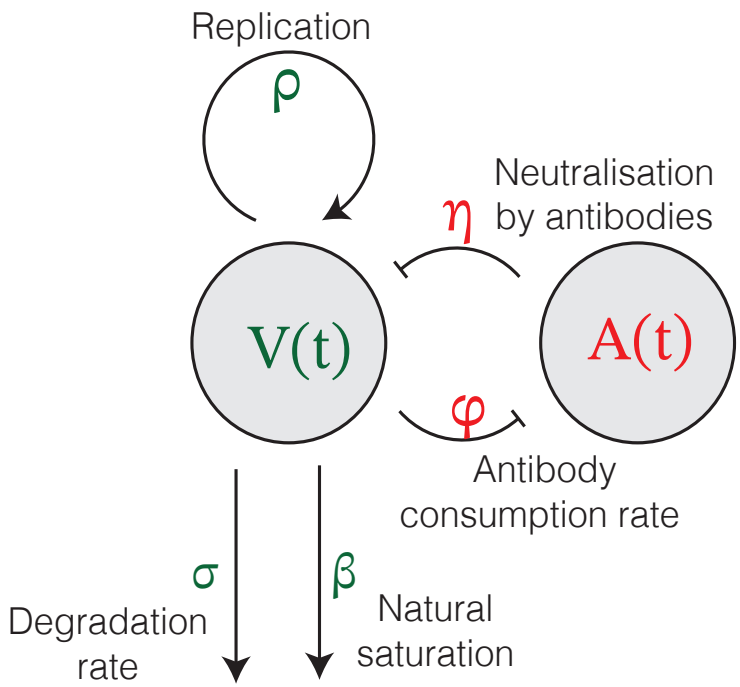

Figure 2. Flowchart of influenza kinetics in the presence of neutralizing antibodies. Viral kinetics is determined by limited viral growth, saturated virus neutralization and saturated antibody consumption.

125

126 Regardless of inoculum size, the kinetics of both A/H1N1pdm09 and A/H7N9

127 converged to the same maximal capacity (Fig. 3). Virus replication parameters obtained

128 through combined SSE can fit SC and MC infection assay data of both viruses (Table1),

129 and is used subsequently to examine the role of virus neutralization in viral kinetics. As

130 a sensitivity analysis, we also fitted a model with an eclipse phase to the data (Fig. S1),

131 however, the additional parameter did not substantially improve the fit (Fig. S2, Table

132 S1); Hence, we used Eq. 1 for the remainder of the study.

133

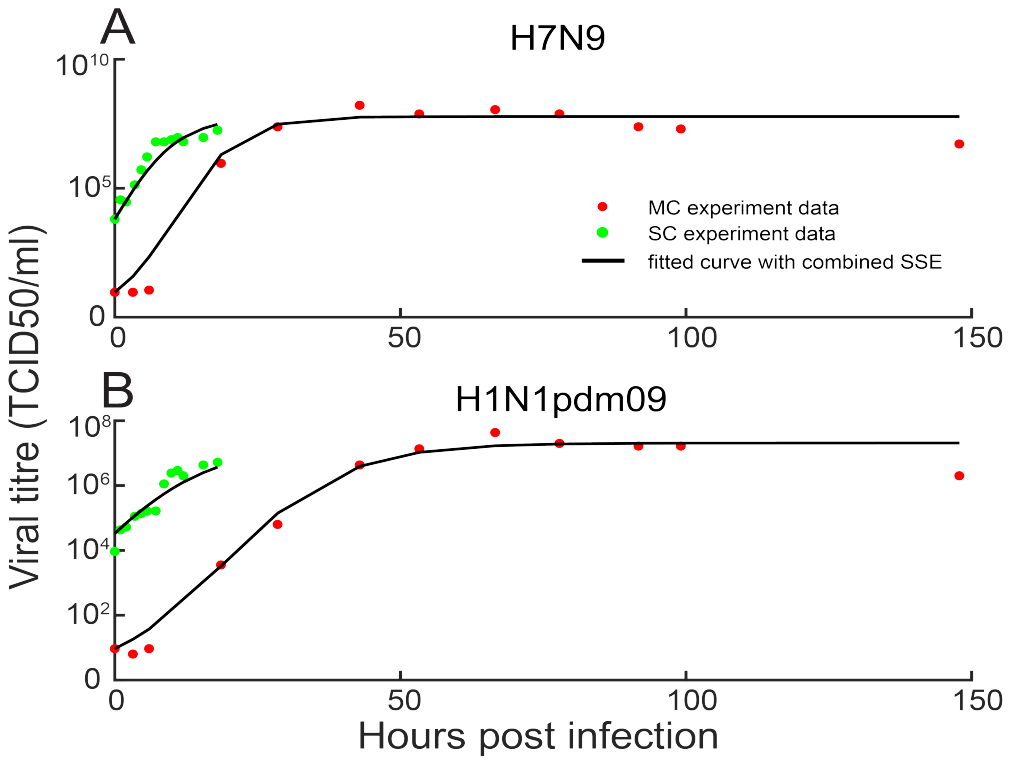

Figure 3. Viral replication kinetics of influenza virus on A549 human lung carcinoma cells. Regardless of viral inoculum sizes, used in single cycle (SC, green) and multi cycle (MC, red) infection assays, both viruses H7N9 (A) and H1N1pdm09 (B) converge to the same maximal capacity. Virus replication parameters were obtained through combined SSE, simulated for 18 hours for the SC assay and 144 hours for MC infection assay. Black curve represents simulated viral replication curve.

Table 1. Estimated parameters of viral replication kinetics (TCID50 scale)

Strain*	Natural birth rate, ρ, (TCID50/ml/hour)	Saturation growth parameter, β, (hour/TCID50/ml)	Natural death rate, σ, (TCID50/ml/hour)	Combined SSE
H1N1pdm09*	1.5555	0.0093	1.4565	3.0821
H7N9*	4.4725	0.0056	4.2857	5.552

*$\rho_0 = 1, \beta_0 = 0.1, \sigma_0 = 1$

Rate of virus neutralization increases but is saturated with increase of both viral titre and antibody concentration.

To establish the quantitative relationship between neutralized virus titre and antibody concentration, we propose a two-dimensional ODE system to fit influenza virus neutralization data estimated from focus reduction assays (FRA) against A/H3N2 virus strains against representative ferret antisera (see methods and Table S2-S18). FRA is routinely used to evaluate neutralizing antibody responses to seasonal influenza viruses, where influenza virus was diluted to a pre-determined concentration, and incubated for one hour with serially diluted ferret antisera generated against representative influenza viruses of the same type. This virus-sera mixture was then added to confluent MDCK-SIAT1 cell lines, allowing the measurement of antibodies required to neutralise virus through reduction of plaques during one-hour incubation.

Since neutralising epitopes are limited on the virus surface, the rate of antibody-virus binding saturates at a concentration higher than or equal to that required for neutralization. Hence, for a fixed viral titre, the rate of virus neutralisation is saturated with increases of antibody (*46*). Similarly, for a fixed antibody concentration saturation also holds for high viral titre. Hence, we describe the rate of change of viral titre and antibody concentration as $\begin{cases} \frac{dV(t)}{dt} = \frac{-\alpha A(t)V(t)}{1+\eta A(t)+\gamma V(t)} \\ \frac{dA(t)}{dt} = \frac{-\varphi A(t)V(t)}{1+\eta A(t)+\gamma V(t)} \end{cases}$, (2). $A(t)$ represents antibody concentration with respect to time t. α represents the rate of virus neutralization by antibody binding; φ represents antibody consumption rate by binding to virus; η controls the saturation in neutralization rate as antibody concentration increases; γ controls the saturation in neutralization rate as viral titre increases. Moreover, by fitting simulated

data with noise following Gaussian distribution $N(0,1)$ of different magnitudes, we found that saturated virus neutralization is more accurate and robust than unsaturated virus neutralization (Section 2.2, *Supplementary material*).

We observed that the virus with antisera grow better than those without antisera for the majority of virus-antisera combination in our FRA assay (Table S2). We hypothesize that this may be due to the presence of virus growth factors in the ferret antiserum, hence, to estimate virus neutralization parameter from FRA we used two approaches: cell control as total viral titre (Section 2.2.1-2.2.3, *Supplementary material*) and viral titre with the most diluted antibody as total viral titre (Table 2 and Section 2.2.4, *Supplementary material*). However, regardless of selection of total titre, the magnitude and category of virus neutralization parameters remain consistent (Section 2.2.1-2.2.3, *Supplementary material*). In the main text, we use viral titre with the most diluted antibody as total titre as example.

Table 2. Estimated virus neutralization parameters (FFU scale)

Dataset	α (ml/FFU/hour)	η (ml/ug)	γ (ml/FFU)	φ (ml/ug/hour)	SSE^*	Category
1	96.8327	0.7788	14.2576	7.167	0.0111	Large
2	24.6437	0.9199	5.2143	0.5620	0.2854	Large
3	3.8399	1.5×10^{-6}	0.6529	2.16×10^{-7}	0.077	Small
4	6.3978	2.44×10^{-7}	0.9358	3.63×10^{-7}	0.0579	Small
5	80.3289	4.5356	1.9437	5.1908	0.2968	Large
6	5.6274	1.45×10^{-6}	1.2741	2.01×10^{-7}	0.3516	Small

*Definition of SSE is given in Materials and Methods.

By fitting System 2 to FRA data collected independently for 51seasonal influenza A/H3N2 viruses collected from individual patients infected during 2014–2019, we found that the estimated virus neutralization parameters of individual viruses can be classified into two categories, with either large (>10^{-2}) or small (<10^{-4}) antibody consumption rates (Figs. 4, S3 and S4, and Tables 2, S11-S14 and S18), however, for most virus-antisera pairs we found that the consumption rate was small (Fig. 4A-D), and these were not based on the specific virus or antisera used in the assay. A comparison of genetic distances between test viruses and viruses used to raise antisera, also showed no apparent relationship with small or large antibody consumption rate (Fig. 4E). For example, a low antibody consumption rate was observed for A/Brisbane/32/2017 against antisera raised against cell-grown A/Kansas/14/2017, while a large antibody consumption rate was observed against egg-grown Kansas/14/2017 (Table 2). However, we found a positive correlation between antibody saturation ($log10(\eta)$) and antibody consumption ($log10(\varphi)$) (Pearson correlation coefficient, 0.7601) and between virus neutralization ($log10(\alpha)$) and antibody consumption ($log10(\varphi)$) (correlation coefficient, 0.7770), showing that the more efficient the antibody is, the more antibody is consumed. These results suggest that, during natural infection antibodies with low antibody consumption rate (i.e. single-hit) will likely lead to better viral clearance due to rapid increases in production of antibodies.

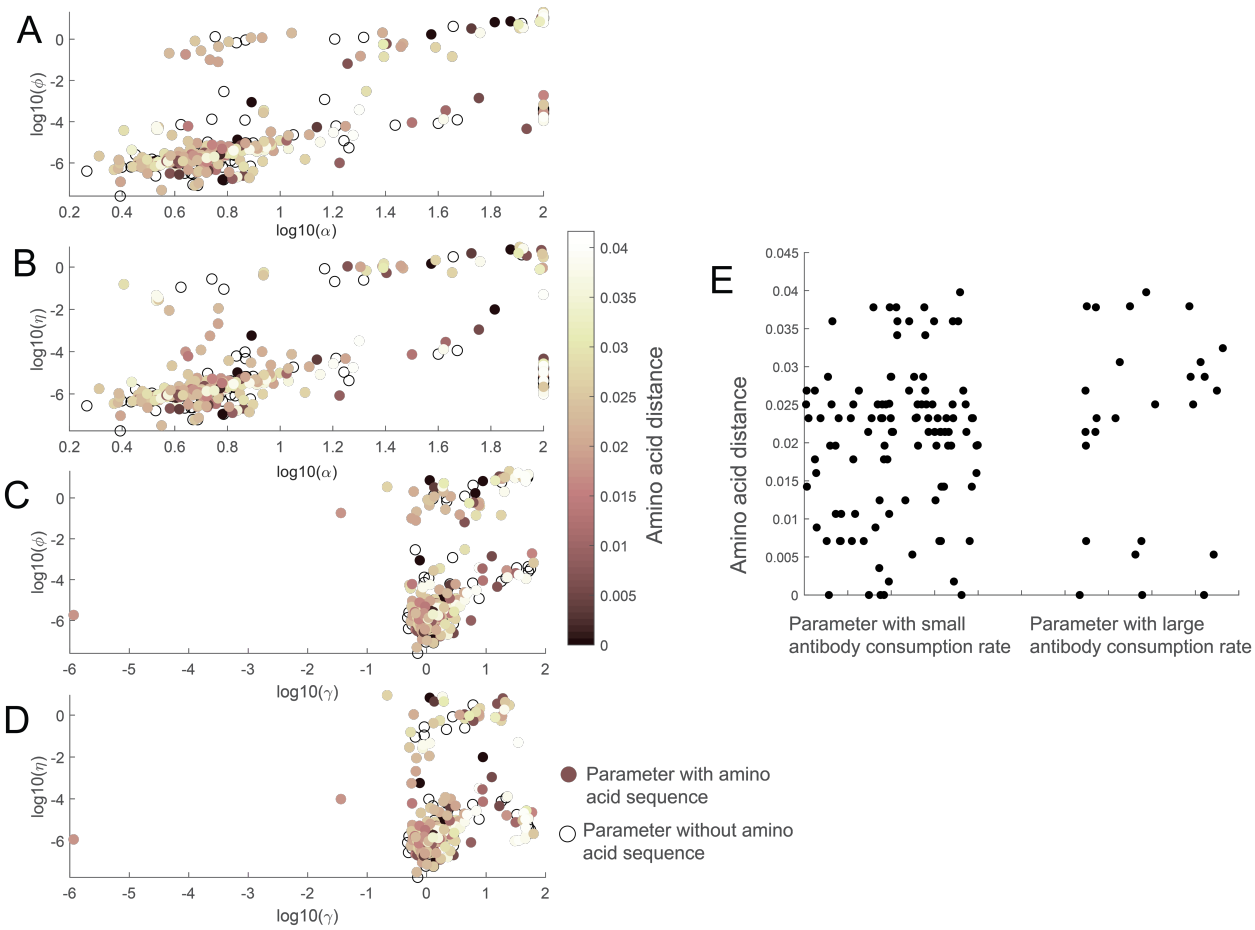

Figure 4. Antibody saturation and antibody consumption are strongly positively correlated. Virus neutralization parameter can be classified into two categories, large and small antibody consumption rate, A) and C). A) $log_{10}(\alpha)$ is plotted against $log_{10}(\varphi)$; B) $log_{10}(\alpha)$ is plotted against $log_{10}(\eta)$; C) $log_{10}(\gamma)$ is plotted against $log_{10}(\varphi)$; D) $log_{10}(\gamma)$ is plotted against $log_{10}(\eta)$; E) Distribution of FRA data of 36 tested influenza virus by HA amino acid distance. Mean and standard deviation of rate of virus neutralization $log_{10}(\alpha)$ are 0.8956 and 0.4378; mean and standard deviation of antibody concentration saturation parameter $log_{10}(\eta)$ are -5.0566 and 1.9286; mean and standard deviation of viral titre saturation parameter $log_{10}(\gamma)$ are 0.2304 and 0.6062; mean and standard deviation of antibody consumption rate $log_{10}(\varphi)$ are -4.6571 and 2.2400.

Antibody-induced bistable viral kinetics exists. To investigate the effects of saturated virus neutralization on viral kinetics in the presence of both susceptible cells and antibodies, we combined Systems 1 and 2:

$$\begin{cases} \frac{dV(t)}{dt} = \frac{\rho V(t)}{1+\beta V(t)} - \sigma V(t) - \frac{\alpha A(t)V(t)}{1+\eta A(t)+\gamma V(t)} \\ \frac{dA(t)}{dt} = \frac{-\varphi A(t)V(t)}{1+\eta A(t)+\gamma V(t)} \end{cases}, (3)$$, and to demonstrate the existence of bistable virus growth kinetics in the presence of neutralizing antibody we simulate System 3 using the parameters estimated in the previous two sections (see above).

In simulations of System 3 with neutralization parameter with small antibody consumption rate (Table S18) and A/H7N9 virus replication parameter, we found the existence of two thresholds A_1 and A_2 that divide the antibody concentration interval into three regimes, shown as bifurcation diagram (Fig. 5E). In different antibody concentration intervals, viral kinetics exhibits different dynamical behaviours. Virus kinetics exhibit bistability at the antibody concentration interval between A_1 and A_2, where small viral inocula are inhibited, and large viral inocula survive under the same antibody concentration. The viral inoculum threshold (above which the virus survives) increases with increase of antibody concentration, shown by the red dashed curve in Fig. 5E. For example, at low antibody concentration $A = 0.075\, ug/ml$, virus with inoculum $10^{1.2} TCID\, 50/ml$, $10^{1.6} TCID\, 50/ml$ and $10^{2.0} TCID\, 50/ml$ survive (Fig. 5B and 5E), whereas at high antibody concentration $A = 0.085\, ug/ml$, virus with high inoculum $10^{1.6} TCID\, 50/ml$ and $10^{2.0} TCID\, 50/ml$ survives (Fig. 5C and 5E). At antibody concentration less than the threshold A_1, the virus survives independent of inoculum (Fig. 5A and 5E), and at antibody concentration higher than the threshold A_2, the virus is inhibited independent of inoculum size (Fig. 5D and 5E).

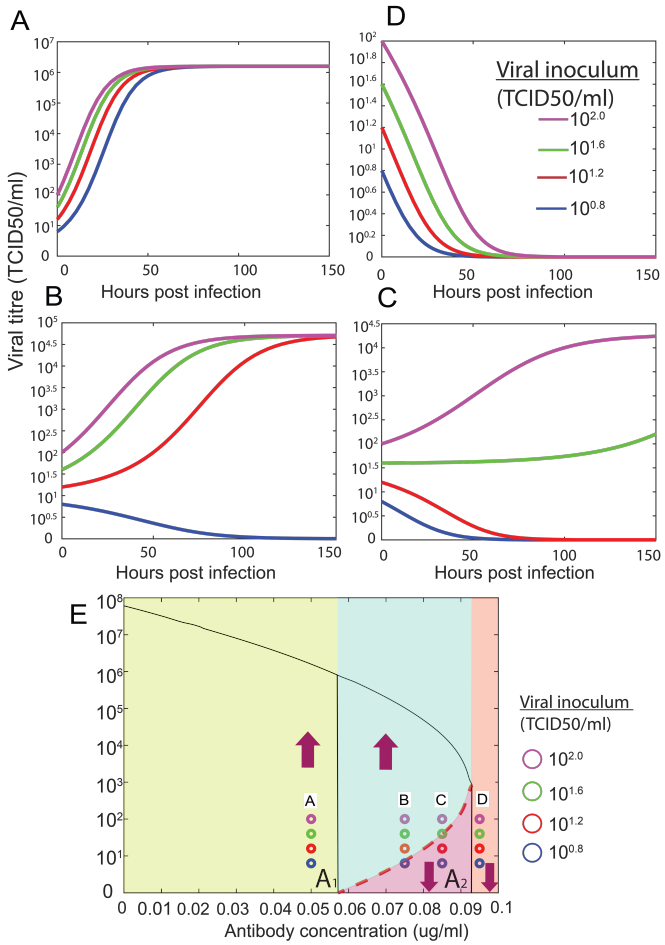

Figure 5. Simulated kinetics of H7N9 virus with different combinations of inoculum sizes and antibody concentrations with low antibody consumption (dataset 3). Bifurcation diagram (E) showing viral titre as a function of antibody concentration. Viral inoculum threshold increases with increase of antibody concentration (red dashed curve). The maximal capacity of viral titre decreases with increases of antibody concentration (black solid curve). Purple arrows represent any viral inoculum size. A) When antibody concentration is between 0 and A_1 virus with any viral inoculum survive. B) Virus with any inoculum size is inhibited when antibody concentration is greater than A_2. C) and D) when antibody concentration is between A_1 and A_2 virus survives if viral inoculum is above dashed red curve and is inhibited if viral inoculum is below dashed red curve. Purple, green, red and blue lines and circles represent viral kinetics with viral inoculum $10^{0.8}$, $10^{1.2}$, $10^{1.6}$ and $10^{2.0}$ TCID50/ml in A–D, also shown as virus inoculum in E.

A similar bistable behaviour was also observed for the replication and neutralization parameters of H7N9 virus estimated with large antibody consumption rate (Table S18) (Fig. 6). With initial antibody concentration $A_0 = 0.04\,ug/ml$, virus with inoculum $10^{1.6} TCID\ 50/ml$ and $10^{2.0} TCID\ 50/ml$ survives, while antibody is depleted

(Figs. 6B, E and S6). With initial antibody concentration $A_0 = 0.05\,ug/ml$, only virus with inoculum $10^{2.0} TCID\ 50/ml$ survives (Figs. 6C, E and S6). The presence of bistability was consistent regardless of estimation method of virus neutralization parameter (control cell or viral titre with the most diluted antibody as total viral titre).

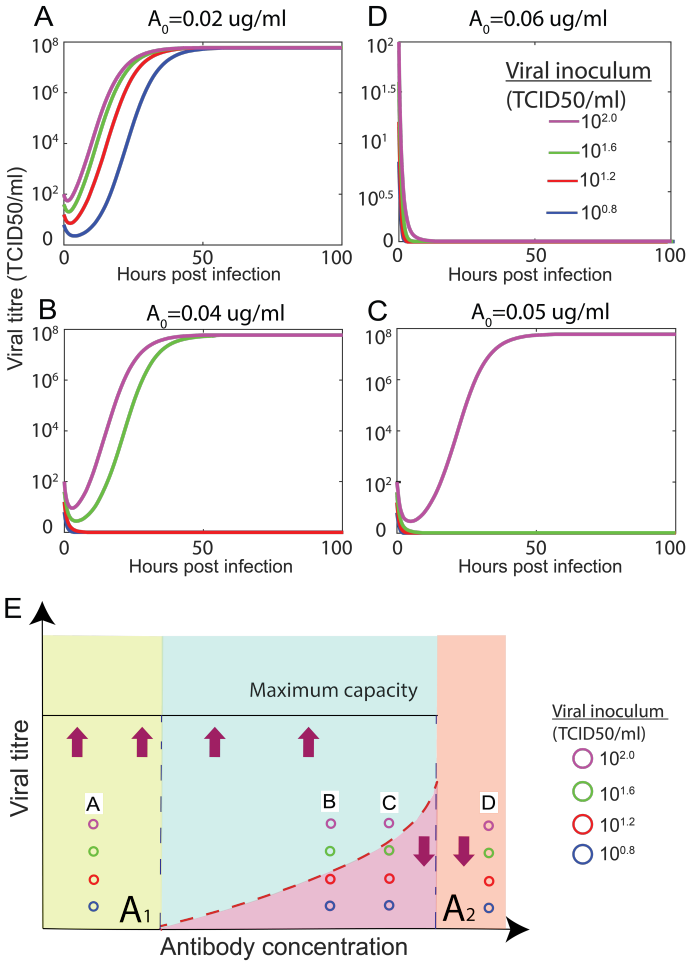

Figure 6. Simulated kinetics of H7N9 virus with different combinations of inoculum sizes and antibody concentrations with high antibody consumption (dataset 2). Viral survival corresponds to antibody depletion and viral eradication coincides with antibody existence. Bifurcation diagram (E) showing viral titre as a function of initial antibody concentration (schematic diagram). Viral inoculum threshold increases with increase of antibody concentration (dashed red line). Maximum capacity of viral titre remains constant if virus survives (black solid line). Purple arrows represent any viral inoculum size. A) When antibody concentration is between 0 and A_1, virus with any viral inoculum survive. B) and C) When antibody concentration is between A_1 and A_2 , viral kinetics survives if viral inoculum is above dashed red curve and is inhibited if viral inoculum is below dashed red curve. D) Virus with any inoculum size is inhibited when antibody concentration is greater than A_2. Purple, green, red and blue lines and circles represent viral kinetics with viral inoculum $10^{0.8}$, $10^{1.2}$, $10^{1.6}$ and $10^{2.0}$ TCID50/ml in A–D, also shown as virus inoculum in E.

226 Although both parameter sets with small and large antibody consumption rates
227 exhibit bistability of H7N9, their behaviour and mechanism are subtly different. For a
228 small antibody consumption rate, exhibited by a majority of FRA data, the antibody
229 concentration during the 144-hour incubation period can be approximated as initial
230 antibody concentration (Fig. S5). In this case, virus and antibody can co-exist at the end
231 of the experiment. Next, the maximum capacity of viral titre decreases with increase of
232 antibody concentration (Fig. 5E). On the other hand, for the few reactions that showed a
233 large antibody consumption, viral survival corresponds to depletion of antibody, while
234 viral eradication coincides with antibody remaining (Figs. 6 and S6). Moreover, both
235 virus titres converged to the same maximum capacity if virus survives in presence of
236 antibody (Fig. 6 and S6). These results were consistent for A/H1N1pdm09 (data not
237 shown).

238 To establish whether bistability depends on model structure, we conducted
239 sensitivity analysis by reintroducing the eclipse phase into the model for A/H7N9, and
240 found that it does not affect existence of bistability and its mechanism (Section 3,
241 *Supplementary material*). We also found the presence of antibody-induced bistable viral
242 kinetics with an eclipse phase introduced in the deterministic model (Section 3.3-3.6,
243 *Supplementary material*). Also, by using the model with unsaturated virus neutralization,
244 we find that the viral kinetics is determined by two categories of virus neutralization
245 parameter, including small and large antibody consumption rate (Table S17, Section
246 2.2.2, *Supplementary material*). For small antibody consumption rate, viral kinetics only
247 exhibits monostability; only antibody concentration determines viral survival and
248 eradication (Fig. S27 and S28, *Supplementary material*). For large antibody

249 consumption rate, viral kinetics exhibits bistability, but antibody concentration interval
250 corresponding to bistability is relatively small (Fig. S29 and S30).

251 We conclude that independent of selection of total viral titre, the magnitude and
252 category of virus neutralization parameter remain consistent. Moreover, regardless of
253 two categories of virus neutralization parameters, antibody-induced bistable viral
254 kinetics always exists; saturated virus neutralization leads to bistability at small antibody
255 consumption rate, while antibody consumption leads to bistability at large antibody
256 consumption rate.

Discussion

We demonstrated that influenza viruses A/H1N1pdm09 and A/H7N9 growing on human cell lines obey our one-dimensional deterministic model and converges to the maximum capacity regardless of viral inoculum sizes. Next, by fitting rates of neutralisation of seasonal influenza A/H3N2 viruses estimated using a focus reduction assay, we have shown that the rate of virus neutralization increases but is saturated with increase of both viral titre and antibody concentration. By integrating estimated viral replication and virus neutralization parameters, we illustrated that antibody-induced bistable viral kinetics universally exists independent of influenza virus strain, absence or presence of eclipse phase, or differences in antibody consumption. Namely, an antibody concentration interval exists where the same antibody concentration can only eliminate small viral inocula but not large viral inocula. Moreover, at this antibody concentration interval, the threshold of viral inoculum above which the virus survives increases with increase of antibody concentration.

Our results imply that even for the same virus-antibody pair, the elimination of virus depends not only on the antibody concentration but also initial virus load (i.e. viral inoculum). Therefore, although the antigenic distance between virus and antibody affects virus neutralization, we suggest that saturated virus neutralization and antibody consumption are biological properties of virus-antibody interactions which lead to variability of virus neutralization independent of antigenic changes. While, viral inoculum size (initial viral load) is the major determinant of survival or death *in vitro*, *in vivo* survival of influenza is determined by factors beyond virus inoculum size, including the time of antibody production and other innate immunity functions. Thus, although

280 antibody concentration and inoculum size are two seemingly important factors, they are
281 not sole contributors for *in vivo* virus eradication. Using influenza antibodies raised in
282 ferrets against seasonal A/H3N2 viruses, we found that the antibody consumption rate
283 could be classified into two categories, viruses with small and large antibody
284 consumption. The variation in antibody consumption may be due to interacting factors,
285 such as binding avidity and affinity, which are well described for influenza. However,
286 importantly, for both antibody consumption categories, our model shows that antibody-
287 induced bistable viral kinetics universally exists independent of influenza virus strain,
288 absence or presence of eclipse phase, or variation in antibody consumption rates.
289 Taken together, these results highlight the important role of virus inoculum size and
290 antibody concentration in the establishment of a successful infection.

291 A second implication of our results is that hemagglutination inhibition (HAI) titres,
292 widely considered as a surrogate marker of protection against influenza infection and
293 hence vaccine efficacy, may not be the only factor influencing protection. Our results
294 imply that for a given HAI titre, whether infection occurred or not, also depends on the
295 virus inoculum size. These results indicate that the quantification of virus inocula which
296 survive or are inhibited for a given antibody for various virus-antisera combinations, to
297 understand the breadth and strength of immune responses, as well as improving
298 vaccine escape and re-infection. These results potentially explain the role of inoculum
299 size in re-infections and low vaccine efficacy in influenza and other viruses, and
300 underlies their complex evolutionary and epidemiological observations.

301 A variety of proposed target cell-infected infected cell-virus (TIV) models of
302 hepatitis B virus (HBV) and simian immunodeficiency virus (SIV) exhibit bistable

303 behaviour, however bistability has been attributed to reversible binding of free antibody
304 (13, 14), which may be biologically unreasonable. Further, these models model virus
305 neutralization as unsaturated, using the mass action term $-\alpha AV$, which is unrealistic as
306 discussed in the Introduction. To our best knowledge, the proposed two-dimensional
307 model is the simplest model with realism leading to bistable switch between viral
308 survival and eradication. By Occam's razor principle, because saturated virus
309 neutralization and antibody concentration is the simplest adequate model, it provides a
310 main underlying mechanism to explain variability of virus neutralization. Besides, without
311 neutralizing antibody, our proposed one-dimensional model can capture viral replication
312 with different viral inoculum sizes. Similarly, by Occam's razor principle, this model is
313 adequate for describing influenza virus replication kinetics on susceptible cells.
314 A limitation of our viral replication kinetics model is that it cannot reproduce
315 observed viral titres when the inoculum is close to the maximum viral load. While
316 A/H1N1pdm09 and A/H7N9 viruses fit our model, the seasonal A/H1N1 (sH1N1) and
317 A/H5N1 data from the same study (42) did not achieve a good fit (data not shown),
318 possibly because the inoculum level is closer to the peak viral load for these data.
319 However, since the viral inoculum in natural infection is considerably low (*12, 15*), our
320 proposed one-dimensional model should be adequate to capture viral kinetics of natural
321 infection. For low inocula, we are confident in our model because for each virus, we
322 fitted the model to data from two inocula simultaneously (0.01 PFU/cell and 3 PFU/cell),
323 and produced good fits for both inocula. Moreover, by using qualitative analysis of
324 ordinary differential equation and delayed differential equation, the long-term behaviours
325 are that virus survives and antibody is depleted. However, we demonstrated that

326 antibody-induced bistable viral kinetics exists within 144 hours because A549 cells used
327 in FRA assays can only survive without fetal calf serum for 144 hours. Additionally, for
328 the case of large antibody consumption rate, the second antibody threshold A_2
329 increases with increase of viral inoculum size. However, because viral inoculum size is
330 limited *in vitro* and *in vivo*, the second antibody threshold A_2 is also limited. Moreover,
331 for large antibody consumption rate, the first antibody threshold A_1 first increases and
332 then decreases with increase of viral inoculum. Thus, schematic diagram of bifurcation
333 diagrams (Fig.6E) provides major information of the whole picture.

334 Using viral replication parameters from one experiment and virus neutralization
335 parameters from another experiment, we have predicted the existence of antibody-
336 induced bistable viral kinetics. To identify the bistable antibody interval for a specific
337 antibody-antigen pair, further work is required to experimentally validate this prediction
338 in a single experimental system. Natural infection can occur with a mixture of virus
339 genotypes (within-host genetic diversity), and the antibody response produced in
340 response to natural infection is polyclonal, hence future modelling with a mixture of
341 genotypes, and protection by polyclonal antibodies is required. Next, in cell-culture
342 experimental system, influenza virus and antibody are co-cultured and then initial
343 inoculum is considered as the initial viral load. However, for *in vivo* experimental
344 system, by the time sufficient antibodies are present to clear infection, the viral load has
345 already been controlled by the innate immune response. Also, our experimental system
346 does not consider variations in growth kinetics in different sites (e.g. nasal vs lung).
347 Further, in our study we used naïve ferret raised antisera where the primary response is
348 known to be narrow, in contrast to humans who exhibit a complex immune history.

349 **Materials and Methods:**

350 **Mathematical models**

351 To investigate the role of antibody concentration and viral inoculum on viral kinetics we
352 developed four models of viral kinetics (a) with antibody consumption (System 3); (b)
353 with antibody consumption and with eclipse phase (System 5, Section 3.2.,
354 *Supplementary Material*); (c) unsaturated virus neutralization (Eq. 6, Section 4,
355 *Supplementary Material*); and (d) unsaturated virus neutralization with eclipse phase
356 (Eq.7, Section 4, *Supplementary Material*). To understand the antigenic relationships
357 among tested H3N2 viruses, we compared the amino acid distance between their
358 hemagglutinin genes (HA) using MEGA X (Molecular Evolutionary Genetics Analysis,
359 https://www.megasoftware.net/). The HA genes of newly generated and reference
360 strains are available in the Global Initiative on Sharing All Influenza Data (GISAID)
361 database (https://www.gisaid.org/). Sequence accession numbers and laboratories
362 generating the sequence data are provided in the Supplementary Materials.

363

364 **Infection assay.**

365 Virus replication parameters were obtained from single cycle (SC) and multiple cycle
366 (MC) infection assays performed by Simon *et al* (42). A549 human lung carcinoma cells
367 were infected with influenza A/H1N1pdm09 (A/Mexico/INDRE4487/2009) and A/H7N9
368 (A/Anhui/1/2013). Both a high viral multiplicity of infection (MOI) (3 PFU/cell) and a low
369 MOI (0.01 PFU/cell) were used. 0.5 mL of the cell supernatant was harvested and
370 frozen at 13 intervals for SC assay that lasted 18 hours (0, 1, 2, 3.5, 4.6, 5.6, 7.1, 8.6,
371 10, 11, 12, 15.5 and 18 hours) whereas 11 intervals (0, 3.1, 18.6, 28.5, 42.9, 53.3, 66.5,

372 77.8, 91.6, 99 and 147) were sampled for MC infection assays that lasted ~150 hours.
373 The frozen samples were thawed and titrated by median tissue culture infectious dose
374 (TCID50) by Simon *et al* (42).
375
376 **Focus Reduction assay.**
377 To determine parameters of virus neutralization we utilized a focus reduction assay
378 (FRA) performed against 13 H3N2 viruses (see below) using post-infection ferret
379 antisera raised against a panel of representative H3N2 viruses. Serial dilutions (80 to
380 10240) of ferret antisera were incubated for one hour with virus and diluted to 1000
381 FFU/well. 100ul of the virus-sera mixture was then applied to confluent MDCK-SIAT
382 cells and incubated for 18-20 hours at 35°C in 5%CO_2. A/H3N2 viruses used in this
383 study include cell-grown A/Hong Kong/4801/2014, cell-grown and egg-grown
384 A/Newcastle/82/2018, cell-grown A/Sydney/22/2018, cell-grown and egg-grown
385 A/Victoria/653/2017, cell-grown and egg-grown A/Switzerland/8060/2017, cell-grown
386 and egg-grown A/Kansas/14/2017, cell-grown A/Tasmania/511/2019, cell-grown
387 A/Tasmania/512/2019, cell-grown A/Tasmania/519/2019, cell-grown
388 A/Canberra/40/2019, cell-grown A/Canberra/61/2019, cell-grown A/Victoria/943/2019,
389 cell-grown A/Darwin/147/2019, cell-grown A/Darwin/148/2019, cell-grown
390 A/Darwin/157/2019, cell-grown A/Darwin/158/2019, cell-grown
391 A/Christchurch/514/2019, cell-grown A/Christchurch/516/2019, cell-grown
392 A/Christchurch/518/2019, cell-grown A/Sydney/1010/2019, cell-grown
393 A/Victoria/23/2019, cell-grown A/Brunei/16/2019, cell-grown A/Canberra/107/2019 , cell-
394 grown A/Canberra/108/2019, cell-grown A/Canberra/109/2019, cell-grown

395 A/Canberra/110/2019, cell-grown A/Fiji/15/2019, cell-grown A/Fiji/25/2019, cell-grown
396 A/Fiji/30/2019, cell-grown A/Fiji/31/2019, cell-grown A/Fiji/36/2019 and
397 A/Brisbane/32/2017. Ferret reference antisera were generated to cell-grown A/Hong
398 Kong/4801/2014, cell-grown and egg-grown A/Newcastle/82/2018, cell-grown
399 A/Sydney/22/2018, cell-grown and egg-grown A/Victoria/653/2017, cell-grown and egg-
400 grown A/Switzerland/8060/2017 and cell-grown and egg-grown A/Kansas/14/2017. FRA
401 was performed for each virus individually with each ferret antisera raised against a
402 representative set of H3N2 viruses. In the main-text, we describe the dynamics using
403 A/Brisbane/32/2017. Following overnight incubation, focus forming units (FFU) were
404 quantified by immunostaining using an anti-nucleoprotein monoclonal antibody and
405 subsequent detection using an HRP-conjugated secondary antibody (BioRad, USA) and
406 TrueBlue substrate (KPL Biosciences). The number of FFU per well was quantified from
407 plate images using an Immunospot analyser and Biospot software (CTL Immunospot,
408 USA). Neutralized virus were estimated by removing FFU count (survived virus) from
409 total virus - we use the average focus number in control wells with virus alone as total
410 virus.
411

412 **Parameter estimation.**

413 Variation in viral replication parameters was estimated using the combined sum of
414 squared error (combined SSE) across the single-cycle and multi-cycle experiments.
415 Combined SSE is $SSE_2 = \sum_{i=1}^{n}\left(log_{10}\left(V_i^{MC}\right) - log_{10}F\left(V_i^{MC}\right)\right)^2 + \sum_{i=1}^{m}\left(log_{10}\left(V_j^{SC}\right) -$
416 $log_{10}F\left(V_j^{SC}\right)\right)^2$, where V_i^{MC} and V_j^{SC} represents experimental viral titer at time i and j. $F(V_i)$
417 and $F\left(V_j\right)$ represent estimated viral titer at time i and j for SC or MC infection assay

data. Initial guesses used for parameter estimation are $\rho_0 = 1$, $\beta_0 = 0.1$, $\sigma_0 = 1$ and $\tau = 0.1$. [#]

For the estimation of virus neutralization parameters, we obtained neutralized influenza virus in one-hour of incubation by using the formula neutralized virus = total virus - survived virus, and selected column with all positive values. Then we calculated neutralized viral titer by the formula, $Viral\ titer = FN \times DR \times SV\ FFU/ml$ where FN represents focus number in each well, DR represents dilution rate, SV represents sample volume and FFU represents focus formation assay. We used the 8 virus serial dilution data points (80 – 12,480) $\{(A_1, V_1), \cdots, (A_8, V_8)\}$ of the FRA, where A_i represents diluted antibody concentration and V_i represents neutralized virus titer. We defined the sum-of-squares error (SSE) as $SSE = \sum_{i=1}^{8}\left(log10(V_i) - log10(F(A_i))\right)^2$, where V_i and $F(A_i)$ represents experimental and theoretical viral titers with respect to the ith diluted antibody concentration. $F(A_i)$ is the integral of $\frac{dV(t)}{dt} = \frac{-\alpha A(t)V(t)}{1+\eta A(t)+\gamma V(t)}$ from 0 to 1.

Qualitative analysis of Mathematical models

By Bendixon-Poincare theorem (19-21), we show non-existence of closed orbits in model systems of viral kinetics with antibody consumption, with and without eclipse phase (System 3 and 5, respectively). The existence of equilibria and its stability for systems with no antibody consumption (Eq. 6 and Eq. 7) is provided by reference (25). The introduction of eclipse phase in System 5 and Eq. 7 does not change the stability of equilibria provided by System 3 and Eq. 6, respectively, as shown by Rouche's Theorem and the continuity of eclipse phase τ (47).

Acknowledgements:

We acknowledge the technical support and advice of Dr. Brendan Russ, Dr. Claerwen Jones, Dr. Jasmine Li and Prof. Zhongfang Wang. S.X and D.V. are supported by contract HHSN272201400006C from the National Institute of Allergy and Infectious Diseases, National Institutes of Health, U.S. Department of Health and Human Services, USA; A.W.C.Y. is supported by a Wellcome Trust Collaborative Award (200187/Z/15/Z); C.M.D is supported by an Australian National Health and Medical Research Council Early Career Fellowship (1113269). The Melbourne WHO Collaborating Centre for Reference and Research on Influenza is supported by the Australian Government Department of Health.

Competing Interests:

The authors declare no conflict of interest.

References:

1. V. N. Petrova, C. A. Russell, The evolution of seasonal influenza viruses. *Nat Rev Microbiol* **16**, 47-60 (2018).
2. S. Cobey, S. E. Hensley, Immune history and influenza virus susceptibility. *Curr Opin Virol* **22**, 105-111 (2017).
3. R. D. Kouyos *et al.*, Tracing HIV-1 strains that imprint broadly neutralizing antibody responses. *Nature* **561**, 406-410 (2018).
4. N. M. Archin, J. M. Sung, C. Garrido, N. Soriano-Sarabia, D. M. Margolis, Eradicating HIV-1 infection: seeking to clear a persistent pathogen. *Nature Reviews Microbiology* **12**, 750 (2014).
5. M. Law *et al.*, Broadly neutralizing antibodies protect against hepatitis C virus quasispecies challenge. *Nature Medicine* **14**, 25-27 (2008).
6. R. B. S. Roden, P. L. Stern, Opportunities and challenges for human papillomavirus vaccination in cancer. *Nature Reviews Cancer* **18**, 240 (2018).
7. G. A. Marsh, R. Hatami, P. Palese, Specific residues of the influenza A virus hemagglutinin viral RNA are important for efficient packaging into budding virions. *J Virol* **81**, 9727-9736 (2007).
8. H. P. Taylor, S. J. Armstrong, N. J. Dimmock, Quantitative relationships between an influenza virus and neutralizing antibody. *Virology* **159**, 288-298 (1987).
9. L. A. VanBlargan, L. Goo, T. C. Pierson, Deconstructing the Antiviral Neutralizing-Antibody Response: Implications for Vaccine Development and Immunity. *Microbiology and Molecular Biology Reviews* **80**, 989-1010 (2016).
10. M. A. Nowak, R. M. May, *Virus dynamics : mathematical principles of immunology and virology*. (2004).
11. A. W. Yan *et al.*, Modelling cross-reactivity and memory in the cellular adaptive immune response to influenza infection in the host. *J Theor Biol* **413**, 34-49 (2017).
12. P. Baccam, C. Beauchemin, C. A. Macken, F. G. Hayden, A. S. Perelson, Kinetics of influenza A virus infection in humans. *J Virol* **80**, 7590-7599 (2006).
13. S. M. Ciupe, C. J. Miller, J. E. Forde, A Bistable Switch in Virus Dynamics Can Explain the Differences in Disease Outcome Following SIV Infections in Rhesus Macaques. *Frontiers in Microbiology* **9**, (2018).
14. S. M. Ciupe, R. M. Ribeiro, A. S. Perelson, Antibody Responses during Hepatitis B Viral Infection. *PLOS Computational Biology* **10**, e1003730 (2014).
15. C. Hadjichrysanthou *et al.*, Understanding the within-host dynamics of influenza A virus: from theory to clinical implications. *J R Soc Interface* **13**, (2016).
16. D. Osthus, K. S. Hickmann, P. C. Caragea, D. Higdon, S. Y. Del Valle, Forecasting seasonal influenza with a state-space SIR model. *Ann Appl Stat* **11**, 202-224 (2017).
17. B. J. Coburn, B. G. Wagner, S. Blower, Modeling influenza epidemics and pandemics: insights into the future of swine flu (H1N1). *BMC Med* **7**, 30-30 (2009).
18. P. Cao *et al.*, On the Role of CD8(+) T Cells in Determining Recovery Time from Influenza Virus Infection. *Front Immunol* **7**, 611 (2016).
19. J. D. Murray, *Mathematical Biology*. (Springer New York, 1993).
20. S. H. Strogatz, *Nonlinear Dynamics And Chaos*. (Sarat Book House, 2007).
21. F. Brauer, C. Castillo-Chávez, *Mathematical models in population biology and epidemiology*. (Springer, New York, NY, 2012).
22. R. Malka, B. Wolach, R. Gavrieli, E. Shochat, V. Rom-Kedar, Evidence for bistable bacteria-neutrophil interaction and its clinical implications. *J Clin Invest* **122**, 3002-3011 (2012).
23. R. Malka, E. Shochat, V. Rom-Kedar, Bistability and bacterial infections. *PLoS One* **5**, e10010 (2010).

24. N. Frenkel, R. Saar Dover, E. Titon, Y. Shai, V. Rom-Kedar, Bistable bacterial growth dynamics in the presence of antimicrobial agents. *bioRxiv*, (2018).
25. R. Malka, V. Rom-Kedar, Bacteria–Phagocytes Dynamics, Axiomatic Modelling and Mass-Action Kinetics. *Mathematical Biosciences and Engineering* **8**, 475 - 502 (2011).
26. T. Francis, On the Doctrine of Original Antigenic Sin. *Proceedings of the American Philosophical Society* **104**, 572-578 (1960).
27. J. Lessler *et al.*, Evidence for antigenic seniority in influenza A (H3N2) antibody responses in southern China. *PLoS Pathog* **8**, e1002802 (2012).
28. J. Ma, J. Dushoff, D. J. D. Earn, Age-specific mortality risk from pandemic influenza. *Journal of Theoretical Biology* **288**, 29-34 (2011).
29. C. Henry, A. E. Palm, F. Krammer, P. C. Wilson, From Original Antigenic Sin to the Universal Influenza Virus Vaccine. *Trends Immunol* **39**, 70-79 (2018).
30. P. Sah *et al.*, Future epidemiological and economic impacts of universal influenza vaccines. *Proceedings of the National Academy of Sciences* **116**, 20786-20792 (2019).
31. K. M. Johnson, H. H. Bloom, M. A. Mufson, R. M. Chanock, Natural Reinfection of Adults by Respiratory Syncytial Virus. *New England Journal of Medicine* **267**, 68-72 (1962).
32. F. W. Henderson, A. M. Collier, W. A. Clyde, F. W. Denny, Respiratory-Syncytial-Virus Infections, Reinfections and Immunity. *New England Journal of Medicine* **300**, 530-534 (1979).
33. C. B. Hall, E. E. Walsh, C. E. Long, K. C. Schnabel, Immunity to and Frequency of Reinfection with Respiratory Syncytial Virus. *The Journal of Infectious Diseases* **163**, 693-698 (1991).
34. W. P. Glezen, L. H. Taber, A. L. Frank, J. A. Kasel, Risk of Primary Infection and Reinfection With Respiratory Syncytial Virus. *JAMA Pediatrics* **140**, 543-546 (1986).
35. T. Sonoguchi *et al.*, Reinfection with Influenza A (H2N2, H3N2, and H1N1) Viruses in Soldiers and Students in Japan. *The Journal of Infectious Diseases* **153**, 33-40 (1986).
36. M. J. Memoli *et al.*, Influenza A Reinfection in Sequential Human Challenge: Implications for Protective Immunity and "Universal" Vaccine Development. *Clinical Infectious Diseases*, (2019).
37. F. Krammer *et al.*, Influenza. *Nature Reviews Disease Primers* **4**, 3 (2018).
38. A. D. Iuliano *et al.*, Estimates of global seasonal influenza-associated respiratory mortality: a modelling study. *The Lancet* **391**, 1285-1300 (2018).
39. K. G. Nicholson, R. G. Webster, A. J. Hay, *Textbook of Influenza*. (Blackwell Science, 1998).
40. K. Murphy, C. Weaver, *Janeway's immunobiology*. (2017).
41. X. Chen *et al.*, Host Immune Response to Influenza A Virus Infection. *Frontiers in Immunology* **9**, (2018).
42. P. F. Simon *et al.*, Avian influenza viruses that cause highly virulent infections in humans exhibit distinct replicative properties in contrast to human H1N1 viruses. *Scientific Reports* **6**, 24154 (2016).
43. L. Mohler, D. Flockerzi, H. Sann, U. Reichl, Mathematical model of influenza A virus production in large-scale microcarrier culture. *Biotechnol Bioeng* **90**, 46-58 (2005).
44. A. P. Smith, D. J. Moquin, V. Bernhauerova, A. M. Smith, Influenza Virus Infection Model With Density Dependence Supports Biphasic Viral Decay. *Frontiers in Microbiology* **9**, (2018).
45. I. NÅSell, Extinction and Quasi-stationarity in the Verhulst Logistic Model. *Journal of Theoretical Biology* **211**, 11-27 (2001).
46. M. Knossow *et al.*, Mechanism of neutralization of influenza virus infectivity by antibodies. *Virology* **302**, 294-298 (2002).
47. R. V. Culshaw, S. Ruan, A delay-differential equation model of HIV infection of CD4(+) T-cells. *Math Biosci* **165**, 27-39 (2000).

48. *R. J. Cox, Correlates of protection to influenza virus, where do we go from here? Hum Vaccin Immunother 9, 405-408 (2013).*
49. *M. J. Memoli et al., Evaluation of Antihemagglutinin and Antineuraminidase Antibodies as Correlates of Protection in an Influenza A/H1N1 Virus Healthy Human Challenge Model. mBio 7, e00417-00416 (2016).*